



## IN THIS ISSUE

Page No.

1. L. Liszka, C-F. Enell, and T. Raita  
*Infrasound in the Atmosphere - Towards a New Propagation Model*

## INFRASOUND IN THE ATMOSPHERE - TOWARDS A NEW PROPAGATION MODEL

*Ludwik Liszka, Swedish Institute of Space Physics, Umeå, Sweden*

*Carl-Fredrik Enell and Tero Raita, Sodankylä Geophysical Observatory, FIN-99600 Sodankylä, Finland*

### Introduction

Infrasound's extraordinary propagation capability has been known for almost a century. In 1908 it was found that the low-frequency signal generated by the Tunguska Meteor event travelled more than once around the Earth and was detected by barographs around the world. It is generally assumed that the low-frequency acoustic waves—infrasound, is minimally attenuated in the atmosphere and propagates through reflections in temperature gradients in the upper atmosphere. That propagation mechanism is believed to be analogous to the propagation of radio waves in the atmosphere.

Continuous observations of infrasound started in Sweden 1972. Three arrays in Northern Sweden were later completed with an array in Uppsala. The Uppsala-array was moved in 2006 to Sodankylä, Finland starting the Swedish-Finnish Infrasound Network (SFIN), a co-operative project between the Swedish Institute of Space Physics and the Sodankylä Geophysical Observatory (Fig. 1).

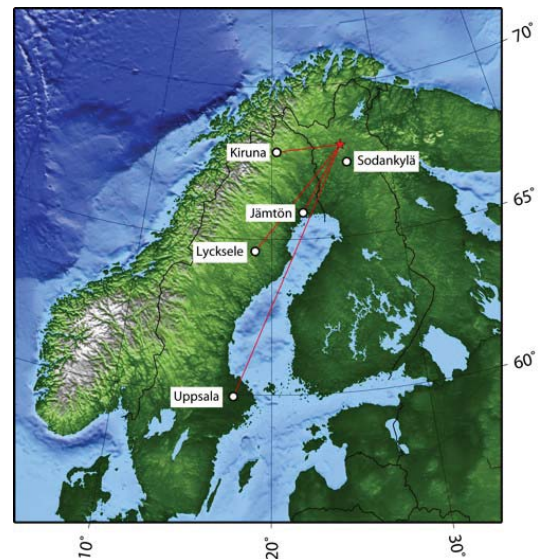


Figure 1: Location of infrasound stations in Sweden and Finland. A star north of Sodankylä indicates location of chemical explosions in Northern Finland.

### INFRAMATICS EDITORIAL BOARD

Michael Hedlin (*Laboratory for Atmospheric Acoustics, UC San Diego*): [hedlin@ucsd.edu](mailto:hedlin@ucsd.edu)

Peter Brown (*University of Western Ontario*): [pbrown@uwo.ca](mailto:pbrown@uwo.ca)

Paola Campus (*Comprehensive Test Ban Treaty Organization*): [paola.campus@ctbto.org](mailto:paola.campus@ctbto.org)

Doug Christie (*Research School of Earth Sciences, Australian National University*): [Douglas.Christie@anu.edu.au](mailto:Douglas.Christie@anu.edu.au)

Milton Garcés (*Infrasound Laboratory, University of Hawaii*): [milton@isla.hawaii.edu](mailto:milton@isla.hawaii.edu)

Alexis Le Pichon (*Commissariat a l'Energie Atomique, DASE*): [alexis.le-pichon@cea.fr](mailto:alexis.le-pichon@cea.fr)

Sergey Kulichkov (*Oboukhov Institute of Atmospheric Physics*): [snk@omega.ifaran.ru](mailto:snk@omega.ifaran.ru)

InfraMatics is an informal series to make available in a timely fashion information about the science of infrasound that any of us might develop. It is provided via our organization's website [www.inframatics.org](http://www.inframatics.org). We expect contributions to InfraMatics to be short and cover only one distinct subject. Figures can be hand-drawn. Lengthy formulae can be stated without derivation. Contributions should be sent to any member of the editorial board by electronic mail. We will assemble all contributions received during a quarter into a single newsletter. The information may be duplicated in the website. We expect that all of us will publish papers that use the material we have previously forwarded to InfraMatics. Everyone is encouraged to do so. To avoid having the material used by someone else in earlier publication, we require that permission to use the material contained in the InfraMatics newsletter by anyone other than the author requires permission by the InfraMatics editorial board. For the time being, Michael Hedlin will act on behalf of the editorial board in such matters.

### 1. The classical propagation model

Although the fact of long distance propagation of low-frequency pressure waves in the atmosphere has long been known, the full explanation, based on experimental data was given for the first time by Procnier and Sharp (1970). They confirmed, using the rocket grenade experiments, air model calculations showing the highest frequency that may be used to reach a given atmospheric height. The results clearly showed lower optimum frequencies toward higher altitudes. This is a result of the increasing high-frequency attenuation with altitude. Long distance propagation (through a reflection in the upper atmosphere) is possible when waves can reach one of the temperature gradients where the reflection takes place. There are two major reflection heights: the temperature gradient in the upper stratosphere (the lower sound channel at 45-50 km) and the temperature gradient in the lower thermosphere (the upper sound channel at 90-100 km).

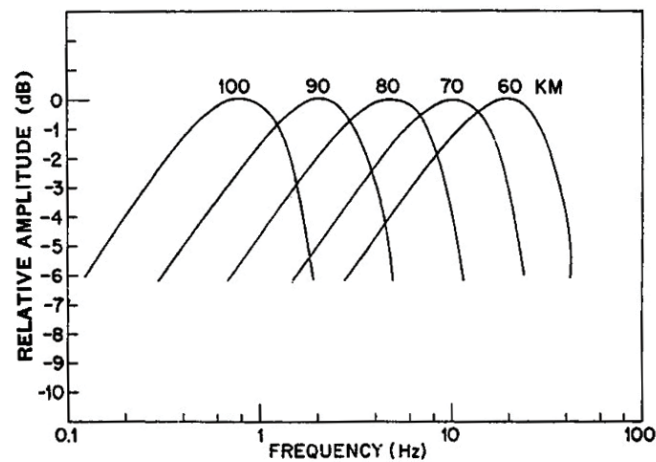


Figure 2: Signal-to-noise ratio for different source heights versus frequency (after Procnier & Sharp, 1970)

When the source is located on the ground, long distance propagation takes place, according to the classical propagation model, only when the signal with given frequency may be detected after reflection in the upper atmosphere at the stratospheric or the thermospheric temperature gradients. It may be seen from Fig. 2 that only signals between 1 and 2 Hz will be detected with the optimal signal-to-noise ratio at the ground after a reflection in the lower thermosphere

(90-100 km). The signal-to-noise ratio is limited at the low frequency side by the atmospheric noise increasing rapidly with the decreasing frequency.

For the above reasons the frequency of 2 Hz was selected for studies of the long distance propagation of infrasound, which started in Kiruna at the beginning of the seventies.

However, a large part of the scientific community still uses frequencies below 2 Hz for detection of distant explosive events. The purpose of the present report is to demonstrate that also frequencies between 2 and 6 Hz may be of interest for long-distance detection.

The propagation of infrasound in the atmosphere is determined by the local refractive index. Since the refractive index depends both on the air temperature (related to the speed of sound) and on the wind vector, height distributions of these two variables determine the propagation of infrasound. An example of the temperature profile is shown in Fig. 3. The temperature profile varies with the geographic position and the time of the year.

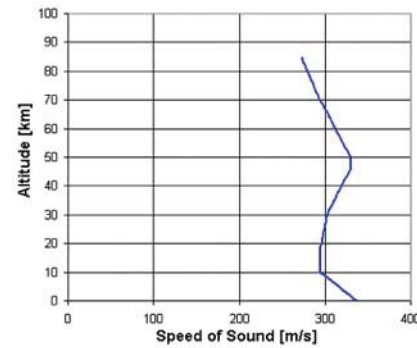


Figure 3. An example of the speed of sound profile

The distribution of wind vector in the atmosphere is quite complex. The wind system varies both with the altitude and it also shows a large temporal variability. Examples are shown in Fig. 4.

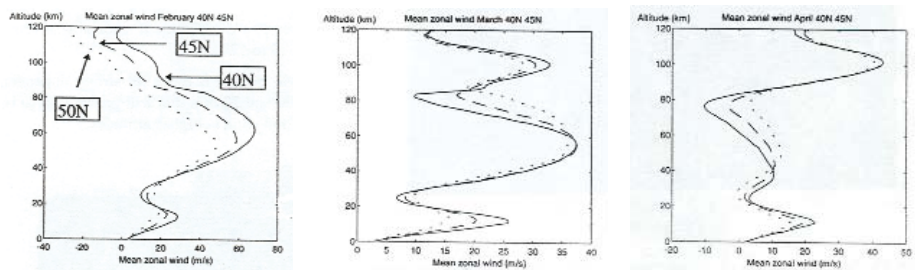


Figure 4. Zonal wind profiles for three different latitudes: 40, 45 and 50N and for three months: February, March and April. Profiles based on COSPAR International Reference Atmosphere 1986.

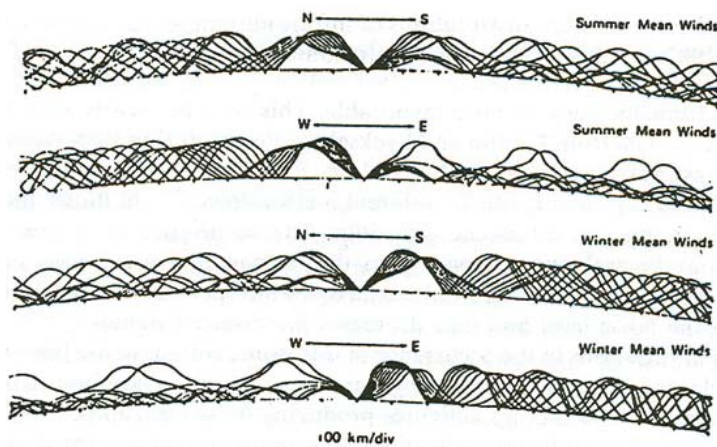


Figure 5. Acoustic ray-paths projected onto vertical east-west plane, for the summer- and winter-mean wind model. Both East-West and North-South propagation is shown. The source is located in the origo (after Georges and Beasley, 1977).

The propagation of infrasound in the atmosphere is studied using the ray-tracing technique. This implies that the medium is divided into thin horizontal layers with a constant refractive index. The dispersion relation for the wave is then solved in each layer, determining the direction of propagation. Examples of propagation of rays launched in different directions and at different time of the year are shown in Fig. 5.

It may be seen that according to the classical propagation model there are considerable zones of silence around the source, where there is no detectable signals.

Already in 1971 attempts were made in Northern Sweden to focus shock-waves from supersonic aircraft either at ionospheric altitudes, or on the ground, after one stratospheric reflection. The calculations of the flight trajectory were made using the ray-tracing calculations based upon either the atmospheric model alone, or the atmospheric model combined with, only few hours old, rocket measurements of wind and temperature. The rocket measurements were made at the near-by rocket range ESRANGE in Kiruna. It has been found that only the ray-tracing calculations, made using the measured (up to 80 km) wind- and temperature profiles, gave a satisfactory focusing of shock-waves.

A considerable amount of efforts has been concentrated on the development of the atmospheric model that would produce ray-tracing result being in agreement with observations. Yet, it has not been possible.

## 2. Difficulties with the classical propagation model

There are several aspects of infrasound propagation that cannot be explained by the classical propagation model. Few of these aspects will be discussed here.

### • Signals from the supersonic vertical re-entry of a rocket

Re-entries of the high-altitude sounding rockets *Castor 4B* and *Skylark 7*, launched at the ESRANGE Space Center outside Kiruna, Sweden, were studied (Liszka, 2008). Observations were performed from three infrasound arrays in northern Sweden, belonging to the Swedish Infrasound Network. The rockets had relatively low entry velocities (2.8 respectively 1.8 km/sec). The fall through the atmosphere was nearly vertical and thus easy to interpret. The *Castor 4B* rocket reaches a height above 700 km while *Skylark 7* only about 250 km. Accurate positioning data for each second of flight was supplied by ESRANGE.

Assuming a model of sound velocity and wind profiles in the atmosphere, which lowest part is adjusted to the closest radiosonde data, it can be seen from ray-tracing calculations (see Fig. 6) that no signal should reach the ground level at a distance corresponding to position of the Kiruna-array. Waves from the upper part of the re-entry would be trapped above the tropopause, while the waves from the lowest part of the re-entry would reach the ground within a 20 km radius from the impact.

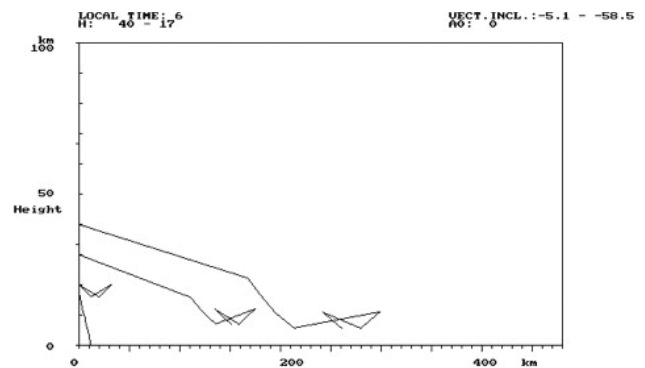


Figure 6. Propagation of sound waves during the descent of a *Castor 4E* rocket. The lowest ray originates at the lowest supersonic altitude of 17 km. All rays originating at heights above 18 km will be dissipated after reflection from the top of the tropopause.

However, all three arrays recorded the re-entry signals in most cases.

• **Signals from chemical explosions at regional distances (<1000 km)**

Destruction of explosives, which took place in Northern Finland (the location indicated with a star on the map of Fig. 1) every summer since 2001, was used as a source of infrasonic signals with known location of the source and the time of origin. The explosions, one or two per day, took place between 07 and 13 UTC. Some results from the summer 2006 were published by Liszka and Kvaerna (2007). There are several properties of recorded signals which are difficult to explain in terms of the classical propagation model.

a) Long duration of the signals recorded at the closest (at that time) infrasonic array in Kiruna, at the distance of 230 km. The signal duration during the entire period August 15-September 15 is shown in Fig. 7.

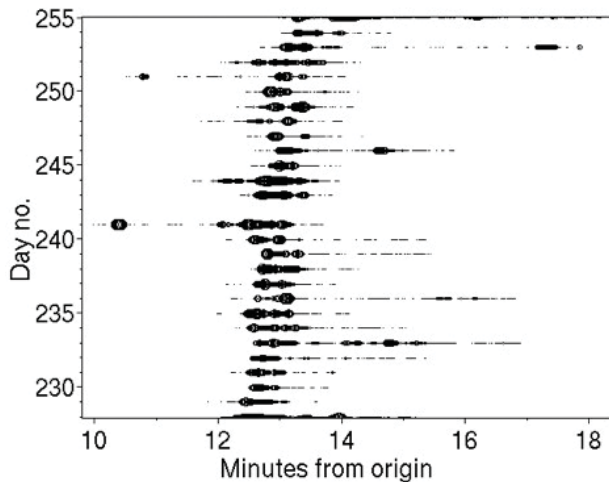


Figure 7. Explosions observed by the Kiruna-array. The time-of-arrival/signal duration is shown. The size of the symbols is proportional to the value of the product  $\rho$  of cross-correlation coefficients across the array.

The duration of the signal as long as up to 5 minutes at that relatively short distance, is difficult to explain, knowing that the source is a single explosion.

b) The distribution of the observed angle-of-arrival is nearly constant up to a distance of about 500 km (Lycksele-array). It may be seen in Fig. 8.

Only the Uppsala-array, at the distance of 980 km, shows the larger spread of the angle-of-arrival (when the signals are recorded there).

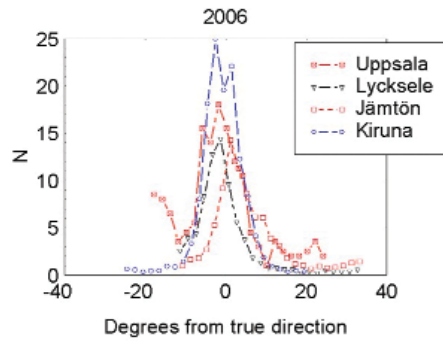


Figure 8. Average distributions of the angle-of-arrival around the true direction to the source for all 4 arrays.

c) Signals recorded at these four arrays do not show clear “arrivals” that could be attributed to reflections at different atmospheric layers (see Fig. 7).

- Detection of signals from distant, relatively weak, sources

Distant artillery shots from a range south of Sodankylä, Finland, were occasionally recorded at all infrasound arrays (except Uppsala) at distances up to almost 500 km. A comparison of observations with current atmospheric conditions will be a subject of a future study. As an example, amplitude recordings från Sodankylä (50 km distance) and

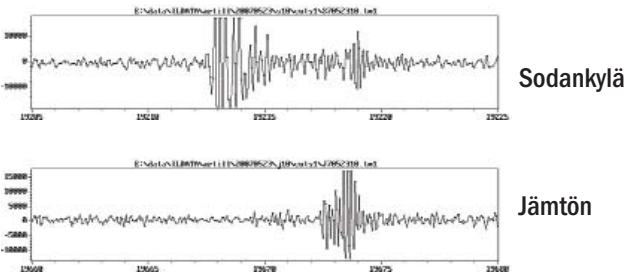


Figure 9. Amplitude recording of the same artillery gun shot in infrasonic signal (caliber 150 mm) from Sodankylä (50 km) and Jämtön (230 km). Amplitudes in arbitrary A/D converter units.

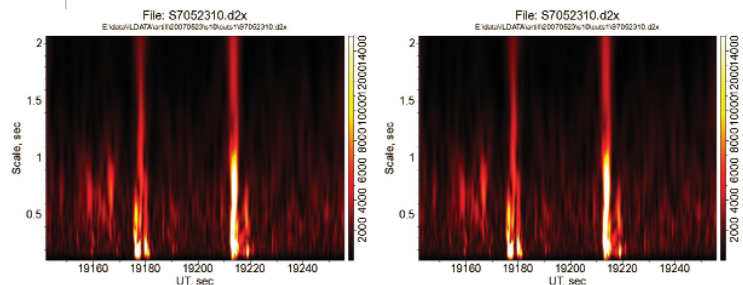


Figure 10. Wavelet spectra (scalograms) of two gun shot signals recorded at distances of 50 km (left) and 230 km (right). The amplitudes of the second signal is shown in Fig. 9.

Jämtön (230 km distance) are shown in Fig. 9.

An interesting conclusion may be drawn from Figs. 9 and 10. It may be seen that, at the distance of 230 km, the signals are dominated by scales around 0.2 sec (5 Hz). These high-frequency signals cannot be propagated through the reflection in the upper sound channel, and thus must be propagated through the troposphere, or at most, through the lower stratosphere.

This observation may be confirmed by the multifrequency analysis (Liszka and Kvaerne, 2007). All array signals are passed through a set of narrow-band wavelet filters and the calculation of the angle-of-arrival and of the trace velocity is performed for each frequency channel. The results for the example of Figs. 8 and 9 are presented in Fig. 11.

It may be seen that at both arrays most of the signals are coming at frequencies 4-5 Hz. At the close array there is also a lot of low-frequency signals arriving from a wide range of azimuths, approximately 20° broad at 1 Hz. The origin of these scattered low-frequency signals will be discussed later. It is plausible to assume that the dominating part of these signals is coming through the troposphere. An important consequence for infrasonic detection will be that these high-frequency **components will be uninfluenced by the stratospheric wind system**. This conclusion is confirmed by the fact that the measured angles-of-arrival at both arrays are 163° and 54.5°, respectively, while the true source azimuths are 162.5° and 54.2°. The existence of tropospherically ducted signals was recently suggested by Negraru and Herrin (2009).

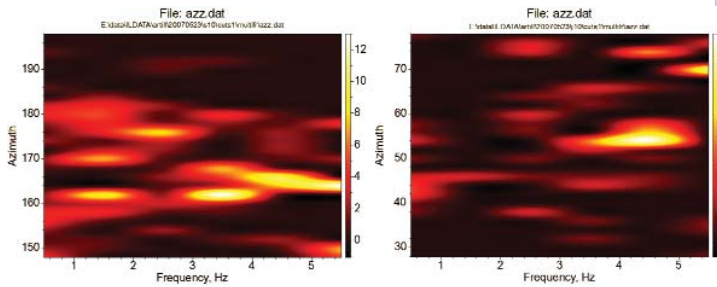


Figure 11. The angle-of-arrival for infrasound from an artillery gun shot as a function of frequency for a close So-dankylä-array (left) and a distant Jämtön-array (right). The intensity scale represents number of readings.

### 3. Atmospheric irregularities—influence on the infrasound propagation

It may be seen from radiosonde measurements, that the temperature, and in particular the wind around the tropopause and in the lower stratosphere show a distinct fine structure, see Fig. 12.

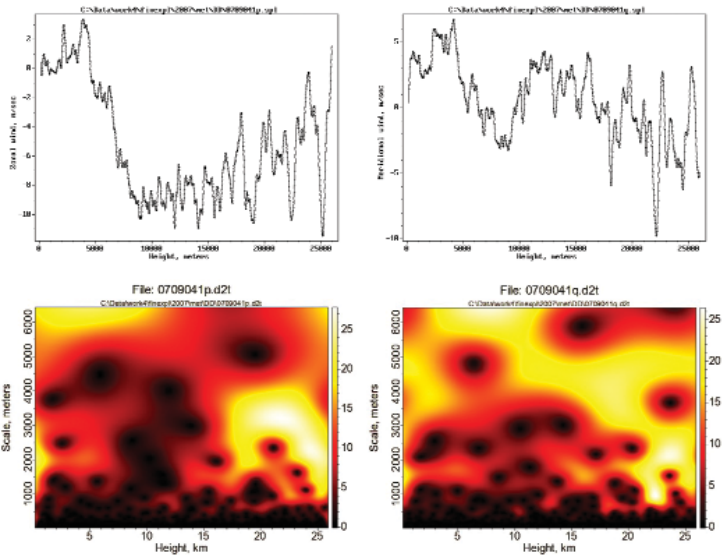


Figure 12. Upper row: Zonal (left) and meridional (right) winds over the Northern Finland (source: Finnish Meteorological Institute) up to 25000 m height on September 4, 2007. Positive direction of the zonal wind is towards W and of the meridional wind towards S.

Lower row: Wavelet scalograms of zonal (left) and meridional (right) winds for the radiosonde data shown in the upper row.

These irregularities may extend both in vertical and in horizontal direction, since with a single radiosonde it is not possible to separate vertical and horizontal irregularities.

Effects of atmospheric irregularities on the propagation of infrasound were discussed earlier by Liszka (1997).

A conventional ray-tracing procedure is based on a 3-D model of the refractive index of the atmosphere,  $n$ , where  $n$  is a function of the sound velocity  $c$  and of the wind vector  $w$ . In order to introduce atmospheric irregularities into the model, it is assumed that, in each point the ray passes, a random term is added to the refractive index calculated from the model. It is assumed that the random term follows a Gaussian distribution. The distribution parameters may be varied. It has been found that even a weak irregularity field superimposed over the model of refractive

index generates semi-regular features in the wave-field. An example is shown in Fig. 13.

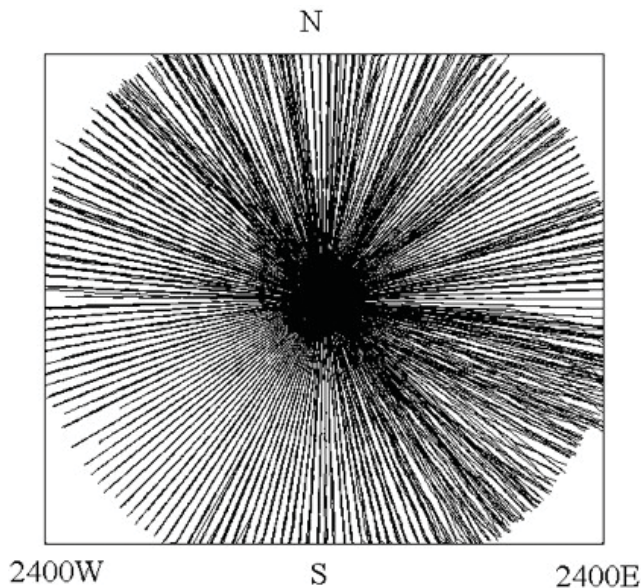


Figure 13. The horizontal projection of rays leaving the source located at origo. The winter wind system is assumed, local midnight and the starting ray inclination  $40^\circ$ . A Gaussian irregularity field with  $\sigma = 0.01$  is superimposed over the wind model.

Bunching up the rays in different directions is clearly visible. The bunching phenomenon disappears when the average magnitude of irregularities reaches a certain level (usually for  $\sigma > 0.02$ ).

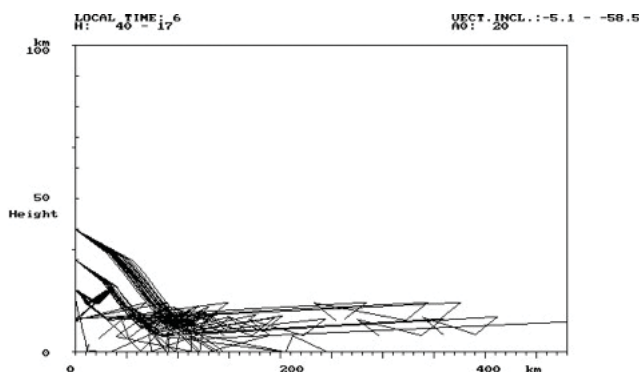


Fig. 14. Propagation of sound waves during the descent of a Castor 4E rocket. The lowest ray originates at the lowest supersonic altitude of 17 km, the atmospheric model with Gaussian-distributed irregularities in wind and temperature is used. A large fraction of the rays that originated at heights above 18 km now reach the ground at distances up to 250 km.

The introduction of irregularities into the atmosphere model also explains the observed signal distribution around the vertical re-entry of a high-altitude rocket (Fig. 14). The signals originated at different heights of the rocket trajectory reach now the ground at large distances from the impact.

In general, the presence of atmospheric irregularities is one of reasons while distinct “silent zones” are never observed at SFIN-arrays.

#### 4. Influence of non-linear effects

The author is indebted to Dr Esko Kyro, Finnish Meteorological Institute for supplying the radiosonde data from Sodankylä.

When dealing with high intensity infrasound waves, as those generated by explosions, it may be expected that non-linear effects will influence the observed wave-field. An interesting phenomenon, which may have a significant effect on observations of distant explosions, was discussed by Stenflo (1987). According to him, high intensity infrasonic waves may generate solitary vortices in the atmosphere.

The infrasound emission from atmospheric vortices was observed by infrasonic arrays in Northern Scandinavia and studied during the recent years (Liszka, 2008). These vortices were found to occur usually in connection with intense weather fronts. There are some indications that these vortices occur in the troposphere, at few kilometres height.

In November 2006 one of arrays was moved to Sodankylä in Northern Finland, only 62 km from the location where the yearly campaign of destruction of explosives takes place. In the summer of 2007 it was found that, during certain meteorological conditions, the arrival of intense infrasonic waves from the explosion site was associated with the simultaneous occurrence of atmospheric vortices overhead of the array. As an example the explosion at 0730 UT on September 4, 2009 is shown in Fig. 15.

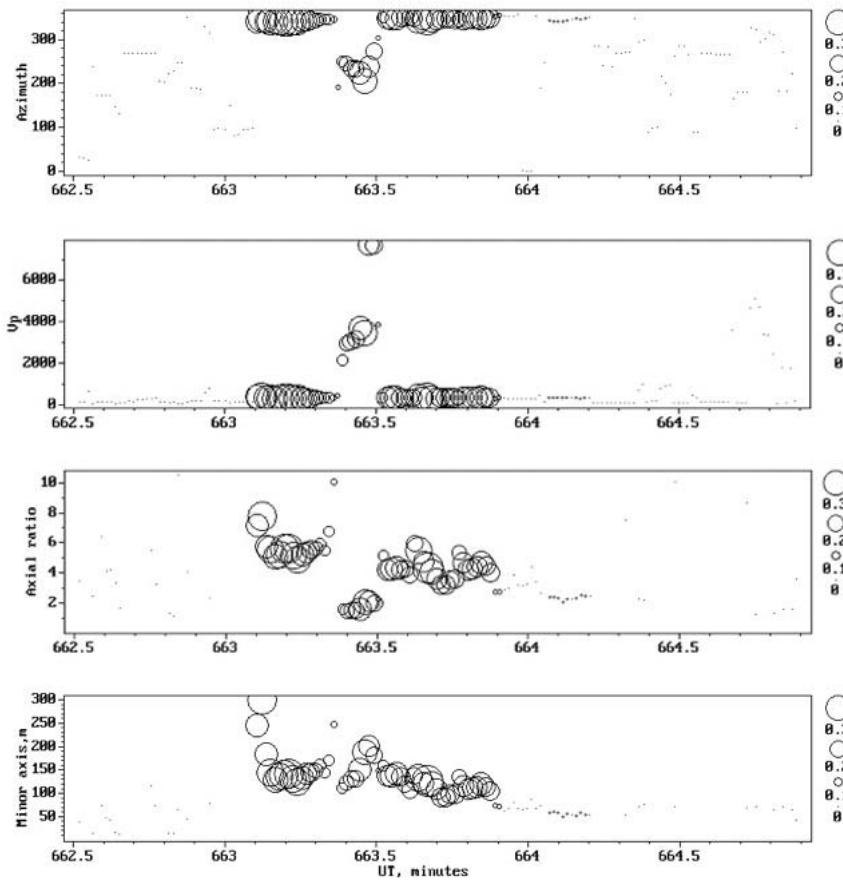


Figure 15. The explosion at 1100 UT on September 3, 2008 recorded at Sodankylä, 62 km from the explosion site. The two uppermost graphs show the angle-of-arrival (graph 1) and the apparent trace velocity (graph 2) across the array. It may be seen that the explosion signal arriving from the true direction of  $338^\circ$  is interrupted by the stronger signal coming from above (very high trace velocity). The frequency content and statistical properties of that signal are identical with frequently observed infrasonic signals from atmospheric vortices. The two lower graphs describe statistical properties of the signal: the axial ratio of the correlation ellipse (graph 3) and the minor axis (in meters) of the correlation ellipse across the array (graph 4). The size of the symbols is proportional to the product of cross-correlation coefficients across the array.

The statistical properties of the intensity pattern across the array may be studied using the technique described by Liszka (2008a). The analysis indicates that the infrasonic waves from atmospheric vortices show different axial ratios of the correlation ellipse than the waves from strong, distant sources. The axial ratio less than 2 is often observed, which means that intensity field from the atmospheric vortices is nearly isometric, unlike the

intensity field from distant sources, where axial ratios larger than 5 are frequently observed. The short correlation distances imply that the large arrays, equipped with large spatial filters, will not be efficient for detection of atmospheric vortices. The correlation ellipses on both sides of the vortex signal shown in Fig. 15 may be plotted on the graph presented in Fig. 16.

Each calculated ellipse is plotted on the xy-plane, with North directed northward. The x-axis is at the same time the time axis (in minutes UTC) and the centre of each ellipse is plotted at the respective time of observation. Since the angle-of-arrival of the explosion signal is  $337^\circ$ , it is apparent that the major axis of each ellipse represents the segment of the wavefront along which the signal is well correlated. It is visible that the correlation ellipse of the vortex signal is close to circular, which means that the signal is well localized.

The arrays belonging to the Swedish-Finnish Infrasonic Network have short distances between the microphones and are equipped with wind barriers instead of spatial filters.

The vortices act as secondary sources of infrasonic in the surrounding of the explosion site. The phenomenon may contribute to the observed distribution of angle-of-arrival shown in Fig. 8.

During the summer 2008 the vortex-infrasonic was associated with at least 50% of explosions observed in Sodankylä.

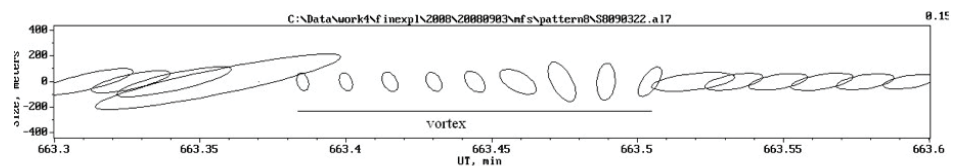


Figure 16. Correlation ellipses plotted on the xy-plane, with North directed northward. The x-axis is at the same time the time axis (in minutes UTC) and the centre of each ellipse is plotted at the respective time of observation.

### 5. Multi-frequency observations of the angle-of-arrival

As indicated earlier, it may be expected that different frequencies in the signal reach the array through different propagation paths. In order to localize the source of infrasound it is necessary to know the true direction to the source, which is, as a rule, not equal to the observed angle-of-arrival of the signal. For a known source it may be of interest to study the difference between the observed angle-of-arrival and the true direction, as a function of signal frequency.

In order to study the statistical properties of the measured angle-of-arrival, the data for each individual detected explosion were analysed in five 1 Hz frequency bands between 1 and 5 Hz. Two variable sets were defined:

1. Difference,  $D$ , between median value of the angle-of-arrival for each frequency and the true source direction.
2. Distribution width,  $W$ , (in degrees) of the angle-of-arrival estimated for each frequency.

The distribution width is defined as the distance between points where number of readings decreases to  $1/e$  of its maximum value. The explosion data analysed for the summers 2006–2008 are shown in Fig. 17 (Kiruna-array), Fig. 18 (Jämtön-array), Fig. 19 (Sodankylä-array—only summers 2007 and 2008) and in Fig. 20 (Lycksele-array—only summers 2006 and 2008).

The vertical scales (colour) on all graphs were optimised with respect to the ranges of measured variables.

The following conclusions may be drawn from the analysis:

- In Kiruna, where the propagation is near to the E-W direction

(85.4°), the difference,  $D$ , for all three summers, is usually negative for lowest frequencies and becomes positive for highest frequencies (upper graphs of Fig. 17). It means that the true angle-of-arrival is usually observed between 3 and 4 Hz. The width of the distribution (lower graphs of Fig. 17),  $W$ , varies from day to day with a preference of larger  $W$  at low frequencies.

- In Jämtön, where the true source direction is 30.8°,  $D$  varies with frequency in opposite way (upper graphs of Fig. 18);  $D$  is positive for lowest frequencies and negative for highest. Also here the large  $W$  is more common at low frequencies.

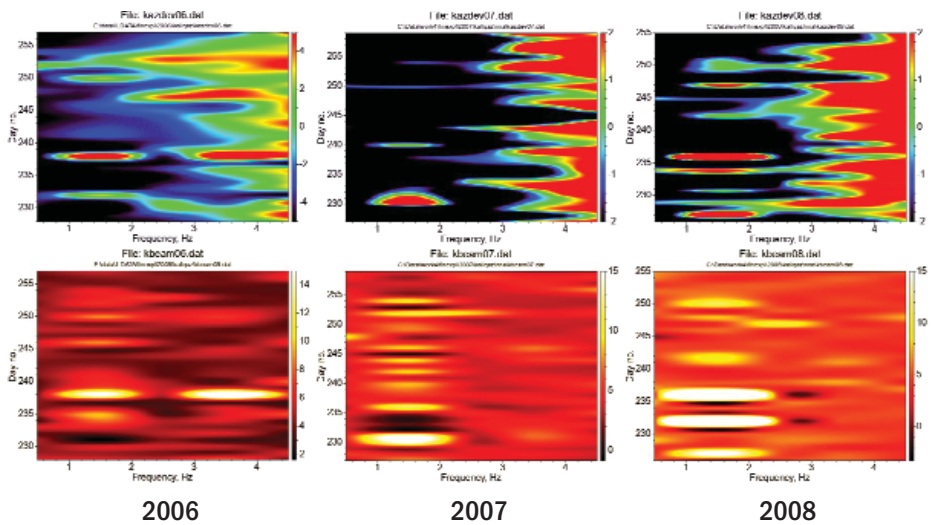


Figure 17. Kiruna- array. The difference in arrival angle,  $D$ , (upper graphs), for all three summers and the width of the distribution (lower graphs),  $W$ , as a function of signal frequency. The vertical axis of each graph shows the day number.

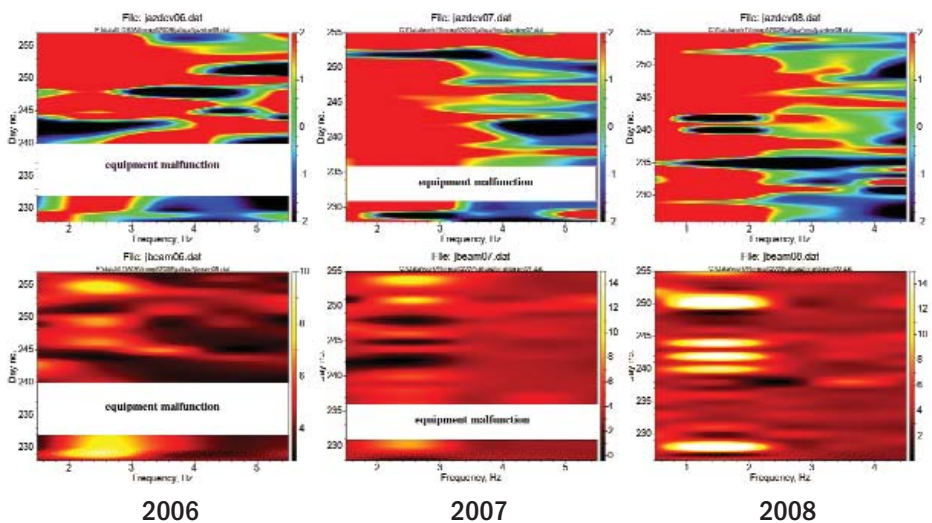


Figure 18. Jämtön- array. The difference  $D$  (upper graphs) for all three summers and the width of the distribution  $W$  (lower graphs) as a function of signal frequency. The vertical axis of each graph shows the day number.

- In Sodankylä, close to the explosion site, there is no visible trend in variations of  $D$  and  $W$  with frequency, see Fig. 19. It is probably due to non-linear effects, like generation of secondary sources around the explosion site.

During August 2006 and 2007 breaks in operation, due to damages caused by lightnings, occurred at the Jämtön-array. Also the Lycksele-array was not in operation during the summer 2007. During the summers 2006 and 2008 the Lycksele-array was in operation, however, no explosion-signals were detected during more than 50% of time. It is probably due to the long distance to the explosion site (487 km).  $D$  and  $W$  computed for days when the explosions were observed in Lycksele don't show any systematic variation with frequency (see Fig. 20).

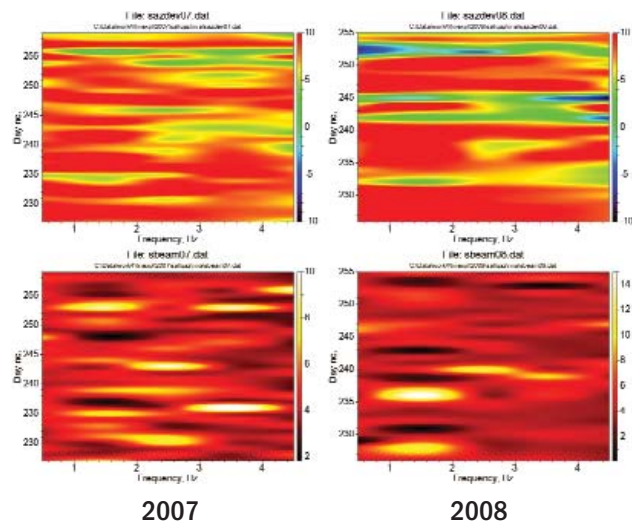


Figure 19. Sodankylä - array. The difference  $D$  (upper graphs) and the width of the distribution  $W$  (lower graphs) for summers 2007 and 2008 as a function of signal frequency. The vertical axis of each graph shows the day number.

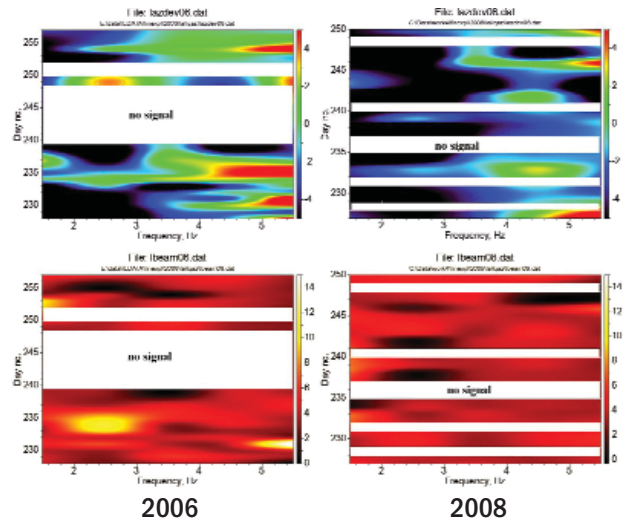


Figure 20. Lycksele - array. The difference  $D$  (upper graphs) and the width of the distribution  $W$  (lower graphs) for summers 2007 and 2008 as a function of signal frequency. The vertical axis of each graph shows the day number.

During the summer 2006 the explosion signals were recorded at few occasions at the Uppsala-array, 978 km from the explosion site. These events were described earlier (Liszka and Kvaerne, 2008).

### 6. Angle-of-arrival and the atmospheric structure below 25 km

A hypothesis was presented in an earlier paper (Liszka and Kvaerne, 2008) that the propagation of the explosion signals seems to be, to a large extent, conditioned by the properties of the atmosphere surrounding the source. The hypothesis is attractive, since if true, the low-altitude (below 25 km) radiosonde data could be used to predict the propagation of the explosion signal. The hypothesis was tested using the daily radiosonde data from Sodankylä, kindly provided by the Finnish Meteorological Institute. The data contains high resolution wind- and temperature measurements up to 25 km altitude. The wind data (magnitude and direction) was converted into the zonal- and meridional components, which could be used in a numerical model. The zonal- and meridional winds above Northern Finland for all three analysed periods are shown in Fig. 21.

The graphs show a remarkable fine structure in the wind system, especially above the tropopause.

### 6.1. MODEL 1

The properties of the angle-of-arrival across the Scandinavia are modelled using a neural network of the back-propagation type. At the first step of modelling the gross structure of the wind and temperature profiles was used. From the original data smoothed values at 1 km step (1-20 km) were obtained using the cubic-spline method. In such way, for each explosion, the atmosphere was described by a 60-component vector (20 readings of the zonal wind, 20 readings of the meridional wind and 20 readings of the sound velocity/temperature). Also relative (measured from the explosion site) latitude and longitude of the observing array were used as inputs to the model. The hidden layer consisted of 70 processing elements. The output of the model consists of 5 pairs of  $D$  and  $W$  (see the previous section), one for each analysed frequency interval between 1 and 5 Hz.

Data from all arrays were used to construct the model.

All data vectors were randomly divided into the learning (80%) and test group (20%).

The network was trained in 150000 steps. The trained network, when used in the recall mode, may visualise trends normally submerged in the noise. Basics of the neural network modelling may be found elsewhere (Liszka 2003).

### 6.2 RESULTS OF MODEL 1

The recall of the Model 1 using the test data showed astonishing results:

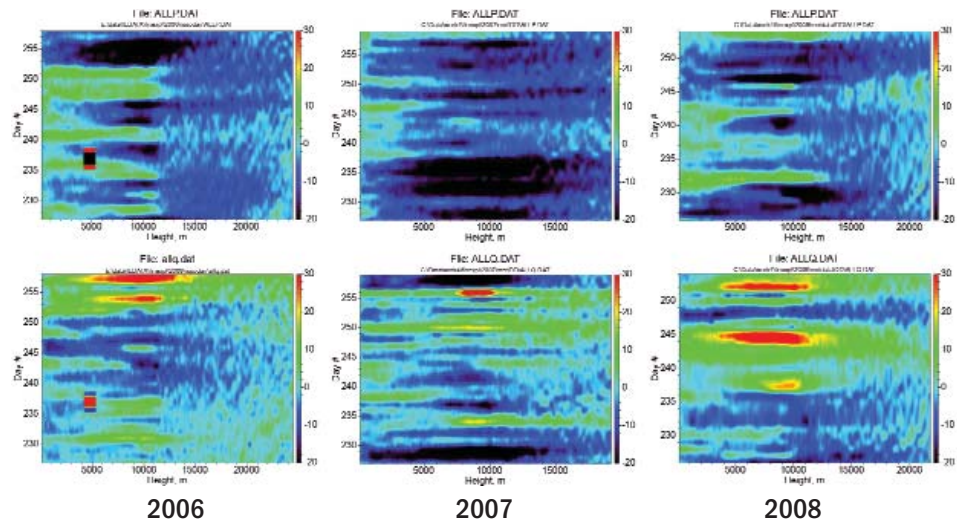


Figure 21. Zonal (upper graphs) and meridional (lower graphs) winds above Northern Finland as a function of altitude for all three analysed summer periods. The vertical axis of each graph shows the day number. The rectangle on day no.237, 2006 is due to missing radiosonde data.

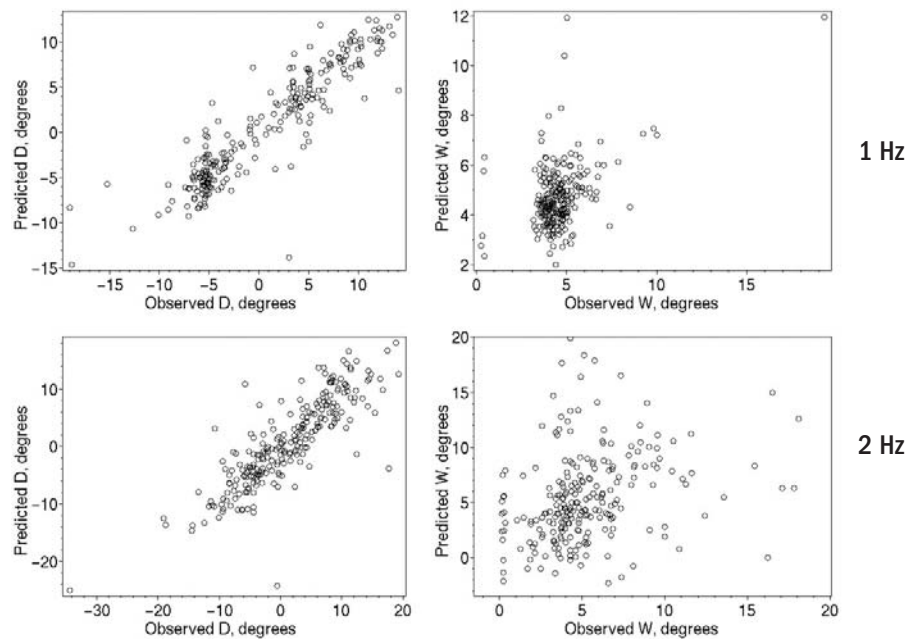


Fig. 22. Predicted differences  $D$  and distribution width  $W$  plotted against their observed values for 1 and 2 Hz frequency channels.

- The difference  $D$  between the observed angle-of-arrival and the true source direction could be predicted from the model with a good accuracy.
- The width  $W$  of the distribution was nearly unrelated to the smoothed atmospheric data used in the model (see Fig. 22)

- The ability of the Model 1 to predict the D was found **highest for 1 Hz** and decreasing with increasing frequency (see Fig 21 showing the predicted D as a function of observed D). The lowest ability to predict the D was observed at 5 Hz (Fig. 23).

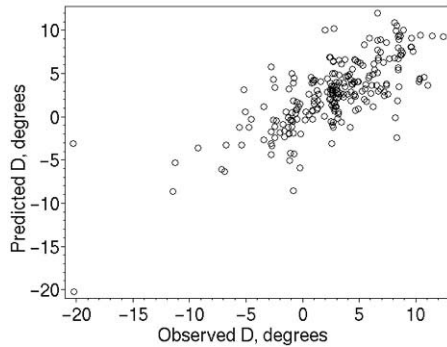


Figure 23. Predicted differences D at 5 Hz plotted against their observed values.

The last observation was unexpected; it is usually assumed that frequencies below 3 Hz propagate through reflections in the uppermost stratosphere and should be related primarily to winds above 20 km. There are, however, indications that, at least at low latitudes, the tropospheric winds may be, to some extent, anti-correlated to the stratospheric winds (K. Mohankumar, Prasanth A. Pillai (2008), Y. H. Zhou, J. L. Chen and D. A. Salstein (2008)).

The results of Model 1 indicate that the radiosonde data may be used as a proxy for the atmospheric wind profile. The model may be used to estimate the difference D at 5 frequencies at given meteorological conditions and then to compute the true angle of arrival.

The remaining question is why the width of the distribution of angle-of-arrival cannot be predicted from the model. One possibility may be that smoothing of altitude profiles removes the information about the fine structure of the atmosphere.

### 6.3. MODEL 2

When infrasound waves are used for the detection purposes, the most important parameter is the detectability of the source, i. e. when the correct angle-of-arrival may be determined. It is illustrated in Fig. 24 showing a comparison of the signal amplitude and of the percentage of time when the correct angle-of-arrival is obtained. The percentage of detection is defined as follows: With the default software settings there are 68 readings of the angle-of-arrival and trace velocity per minute. Readings with a

plausible trace velocity corresponding to the product of all 3 cross-correlation coefficients larger than 0.03 are assumed to be correct. The detectability,  $\Delta$ , (in %) is then:

$$\Delta = N/34 * 100\%$$

Where N is the number of correct readings during a 30 sec period.

It may be seen from Fig. 24 that the correct angle-of-arrival may be determined even for wave amplitudes comparable with the background noise.

An attempt was made to model the detectability at a single array (Kiruna) as a function of radiosonde data, using a neural network model of back-propagation type. The input of the model consists of a 60-component vector created from radiosonde data in the same way as in the Model 1. The model has 70 processing elements in the hidden layer. The output consists of 17-point sequence of detectability starting at 10 minutes after the explosion. The data from explosions during summers 2006-2008 and from the Kiruna-array were used. 80% of data were used for training of the model and the remaining 20% to test the trained model (recall).

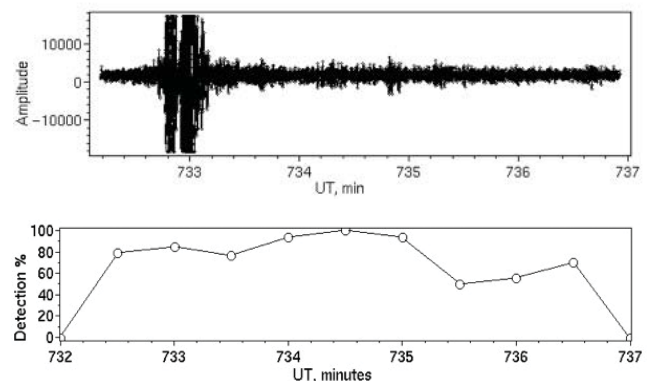


Figure 24 Amplitude recording from Kiruna of the explosion on August 21, 2006 (upper graph) together with the percentage of detection, detectability (lower graph).

Examples of the recall together with the observed detectability are shown in Fig. 25 for 4 explosions.

It may be concluded that in cases when only a single period of signal is detected, like the uppermost case of 2006-09-11, the detectability as a function of time may be predicted with a good accuracy. When the recorded signal

shows complex temporal variations, the predicted detectability also shows a similar structure. However, the predicted secondary maxima tend to occur later than those observed. It must be remembered that the Model 2 was constructed using data from only about 90 explosions. The data from additional 5 summers (2001-2005) will be used for further model development.

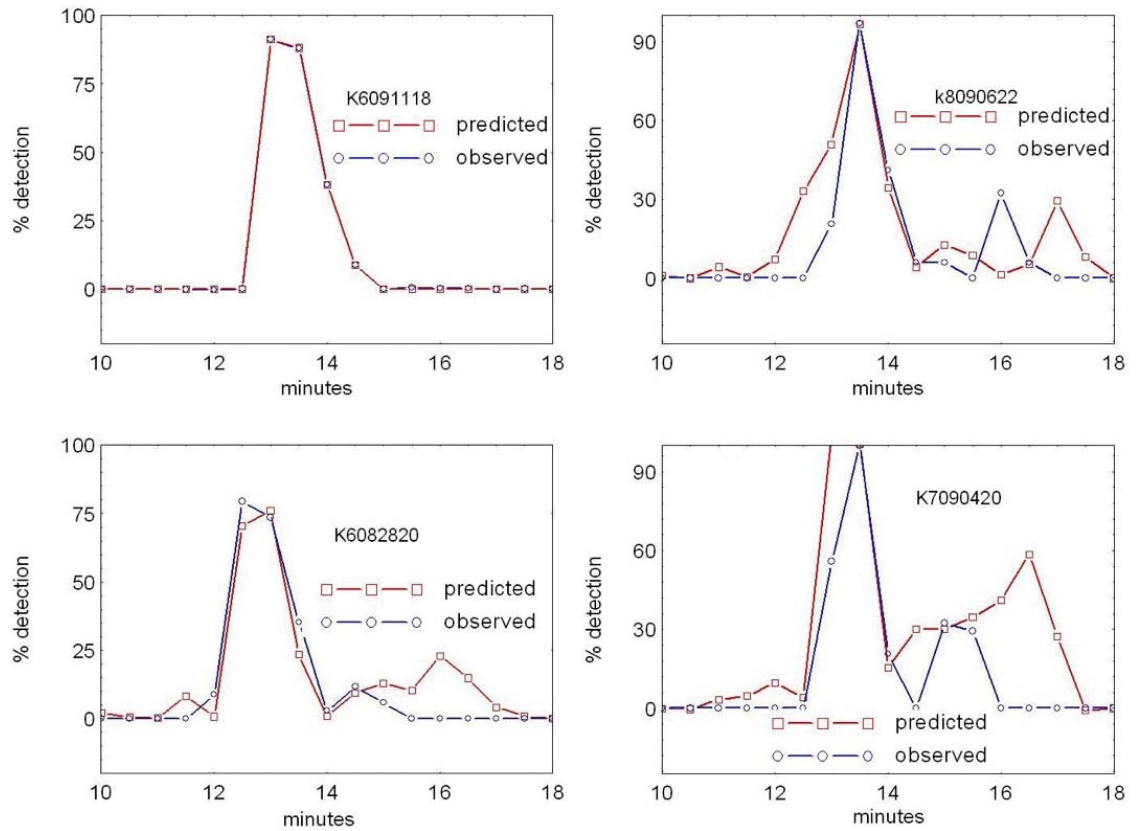


Figure 25. Results of recall of Model 2 (red line) together with observed detectability (blue line) for 4 explosions recorded at the Kiruna-array. The x-axis shows the time (in minutes) elapsed after the explosion.

### 7. The signal detectability and the array dimensions

Not all wave packets reaching the array may be detected.

As it was mentioned in earlier sections the cross-correlation over the array may be described by an ellipse. The minor axis of the ellipse is determined by the dominating frequency of the signal. The major axis is nearly perpendicular to the direction of propagation. The major axis is thus the part of the wave front along which the signal is correlated. The infrasonic waves cannot be visualized as a system of infinite wave fronts.

The correlation distances shorter than a half of the shortest distance between microphones cannot be measured. It has been found that for arrays of the Swedish-Finnish Infrasound Network with the shortest distance between

microphones of 75 meters, correlation lengths down to 40 meters may be determined. In other words the arrays cannot detect small wave packets with correlation distances along the wave fronts shorter than 40 meters.

The major axis of the correlation ellipse is thus a measure of the size of an individual wave packet.

As an example the correlation ellipses for the explosion signal shown in Fig. 24 are shown in Fig. 26. The explosion signal arrives from the direction of 85.4°.

It is possible to simulate arrays with different distances between the microphones by removing readings for wave packets smaller than a given threshold value, characteris-



Figure 26. Correlation ellipses plotted on the xy-plane, with North directed northward. The x-axis is at the same time the time axis (in minutes UTC) and the centre of each ellipse is plotted at the respective time of observation. The explosion of August 21, 2006 recorded in Kiruna. The vertical scale is in meters.

tic for a certain smallest distance between microphones. An example of simulated detectability for the explosion shown in Figs. 24 and 26 and for four different correlation distances is presented in Fig 27.

It is apparent that when the minimum distance between the microphones exceeds 150 meters, the detectability drops and the coherent signal extracted from two microphones starts to show several “arrivals”.

An interesting conclusion may be drawn studying variations of the major axis of the ellipse as a function of time

(Fig. 28). A number of very large values of the major axis are embedded in a continuum of much smaller values. An inspection of the distribution of recorded values of the major axis indicates that the distribution is not uniform and that there is an excess of very large values (>1000 meters). This property of the distribution may be a reason why short bursts of the signal from weak sources may, sometimes, be detected at very long distances.

It is usually assumed that a large size of an array guarantee for the array’s performance. It may be true under assumption that distances between its microphones are kept

short (preferably under 100 meters). No matter which detection principle is used, the large distances between microphones cause that different wave packets, often travelling along different propagation paths, are treated as parts of the same wave front.

### Conclusions and future plans

The present study indicates that an empirical propagation model may be constructed using the meteorological radiosonde data. There is an advantage of using radiosonde data: the radiosonde data are collected at 12 hours intervals at numerous geographical locations. The model can be used to determine the true direction to the source and to predict the temporal structure of the recorded signal.

The primary goal of infrasonic detection is to determine the true angle-of-arrival at least at two arrays. These data may then be used to localize the source. Using the Model 1 it is possible to correct the observed angle-of-arrival at Kiruna and Jämtön and thus to determine the source location. It has been found that, after correction, at the range of distances actual here the source location could be determined with an accuracy of +/- 5 km.

The further development of the model will include prediction of correlation ellipses. It may be expected that properly scaled atmospheric data may be used to determine the shape of the distribution of correlation ellipses. That means that the model could be used to predict the probability of specific correlation distances in

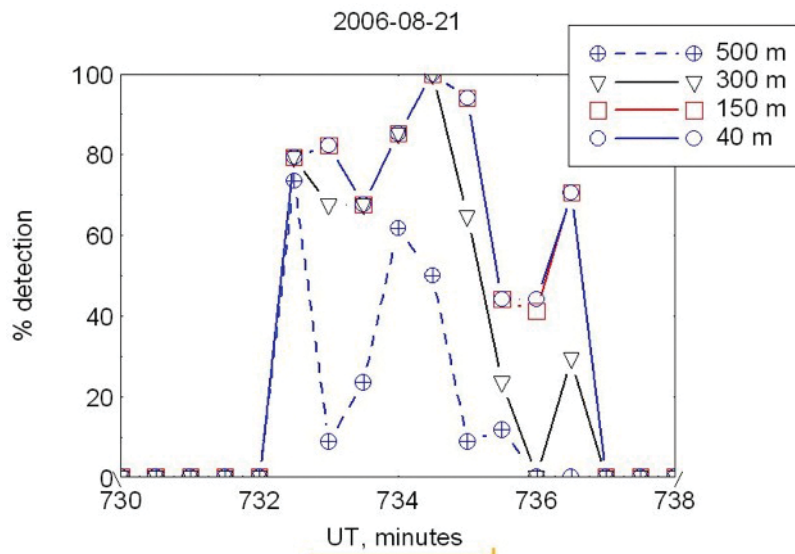


Figure 27. Detectability for the explosion signal recorded in Kiruna on August 21, 2006 for different minimum distances between microphones.

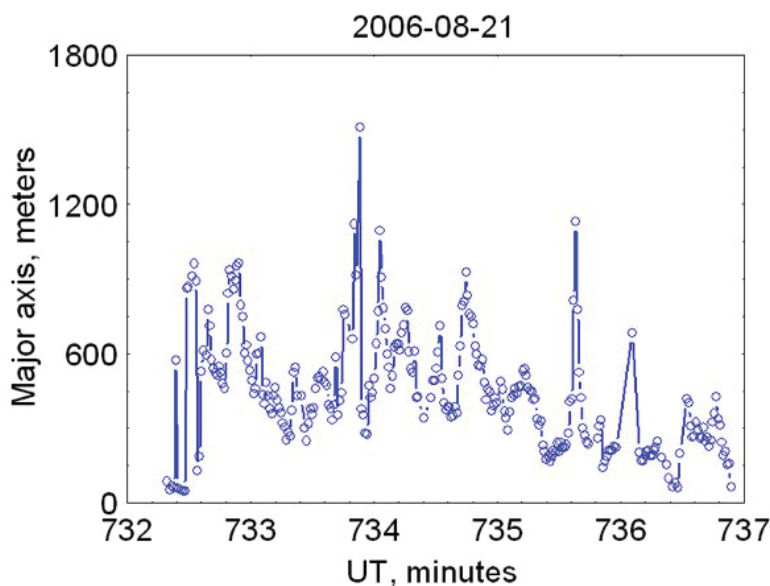


Figure 28. The major axis of the correlation ellipse for the explosion of August 21, 2006 as a function of time.

the wave field, and thus the probability of detection at a given geographical location.

Increasing the size of the network of infrasonic arrays it would be possible to construct a model based on radiosonde data collected at several geographical locations.

### Acknowledgements

The author is indebted to Dr Esko Kyro, Finnish Meteorological Institute for supplying the radiosonde data from Sodankylä.

### References

Georges, and T.M., Beasley, W.H., 1977, Refraction of infrasound by upper-atmospheric winds, *J. Acoust. Soc. Am.*, **61**: 28-34.

Liszka, L. J., 1974, *Acoust. Soc. Am.*, **56**: 1383 (1974).

Liszka, L., 2003, Cognitive Information Processing in Space Physics and Astrophysics, Pachart Publishing House, Tucson, Az, USA, ISBN 0-88126-090-8

Liszka L., 1997, Propagation Effects and Localization of Infrasonic Sources, AGU Fall Meeting, San Francisco.

Liszka, L., 2008, Infrasound - A summary of 35 years of infrasound research. IRF Scientific Report No. 291.

Liszka, L., 2008, Infrasound from Atmospheric Vortices. Paper presented Infrasound Workshop, Bermuda.

Liszka, L. and T. Kvaerna, 2008, Propagation of infrasound from chemical explosions. *Inframatics*, **20**, ([http://www.inframatics.org/pdf/inframatics\\_mar2008.pdf](http://www.inframatics.org/pdf/inframatics_mar2008.pdf))

Negraru, P. and Herrin, E., 2009, On infrasound waveguides and dispersion, *Seismological Research Letters* 80(4): 565-571.

Procunier R. W. and G. W. Sharp, 1971, *J. Acoust. Soc. Am.* **49**: 622.

Stenflo, L., 1987, Acoustic solitary vortices. *Phys. Fluids*, **30** (10): 3297.